Atmos. Chem. Phys. Discuss., 12, 1687–1732, 2012
www.atmos-chem-phys-discuss.net/12/1687/2012/
doi:10.5194/acpd-12-1687-2012

Atmospheric Chemistry and Physics Discussions

Strong sensitivity of aerosol concentrations to convective wet scavenging parameterizations in a global model

B. Croft[1], **J. R. Pierce**[1], **R. V. Martin**[1,2], **C. Hoose**[3], **and U. Lohmann**[4]

[1]Department of Physics and Atmospheric Science, Dalhousie University, Halifax, Canada
[2]Harvard-Smithsonian Center for Astrophysics, Cambridge, MA, USA
[3]Karlsruhe Institute of Technology, Karlsruhe, Germany
[4]Institute of Atmospheric and Climate Science, ETH Zurich, Zurich, Switzerland

Received: 3 January 2012 – Accepted: 10 January 2012 – Published: 19 January 2012

Correspondence to: B. Croft (croft@mathstat.dal.ca)

Published by Copernicus Publications on behalf of the European Geosciences Union.

Abstract

This study examines the influences of assumptions in convective wet scavenging parameterizations on global climate model simulations of aerosol concentrations and wet deposition. To facilitate this study, an explicit representation of the uptake of aerosol mass and number into convective cloud droplets and ice crystals by the processes of activation, collisions, freezing and evaporation is introduced into the ECHAM5-HAM model. This development replaces the prescribed aerosol cloud-droplet-borne/ice-crystal-borne fractions of the standard model. Relative to the standard model, the more consistent treatment between convective aerosol-cloud microphysical processes yields a reduction of aerosol wet removal in mixed liquid and ice phase convective clouds by at least a factor of two, and the global, annual mean aerosol burdens are increased by at least 20 %. Two limiting cases regarding the wet scavenging of entrained aerosols are considered. In the first case, aerosols entering convective clouds at their bases are the only aerosols that are scavenged into cloud droplets, and are susceptible to removal by convective precipitation formation. In the second case, aerosols that are entrained into the cloud above the cloud base layer can activate, can collide with existing cloud droplets and ice crystals, and can subsequently be removed by precipitation formation. The limiting case that allows aerosols entrained above cloud base to become cloud-droplet-borne and ice-crystal-borne reduces the annual and global mean aerosol burdens by 30 % relative to the other limiting case, and yields the closest agreement with global aerosol optical depth retrievals, and black carbon vertical profiles from aircraft campaigns (changes of about one order of magntiude in the upper troposphere). Predicted convective cloud droplet number concentrations are doubled in the tropical middle troposphere when aerosols entrained above cloud base are allowed to activate. These results show that aerosol concentrations and wet deposition predicted in a global model are strongly sensitive to the assumptions made regarding the wet scavenging of aerosols in convective clouds.

ACPD
12, 1687–1732, 2012

1 Introduction

Aerosols play an important role in the climate system by influencing the Earth's radiation budget, directly by scattering and absorbing radiation, and indirectly by modifying cloud properties (Twomey, 1991; Charlson et al., 1992). Aerosols also have important impacts on global air quality (van Donkelaar et al., 2010), and human health (Dockery et al., 1993). As a result, the prediction of three-dimensional aerosol distributions is important in both global climate, and air quality models. These distributions are strongly influenced by convective transport and wet scavenging in convective clouds. However, the representation of convective processes remains a major uncertainty for aerosol prediction in global models (Randall et al., 2003; Lohmann, 2008; Tost et al., 2010).

The parameterization of convective clouds in global models is a subject of ongoing research efforts (Nober et al., 2003; Menon and Rotstayn, 2006; Lohmann, 2008). However, the aerosol-cloud interactions involving convective clouds are complex and difficult to capture in global models (Morales et al., 2011). Aerosols influence convective clouds since they act as cloud condensation and ice nuclei, and also by the semi-direct effect since they absorb radiation, which produces local heating that contributes to cloud dissipation (Hansen et al., 1997; Ackerman et al., 2000). Conversely, convective clouds also influence three-dimensional aerosol distributions by processes such as aerosol wet scavenging and cloud processing (Engström et al., 2008).

Further evidence of the uncertainty related to convective processes in global models is the wide disparity amongst these models in terms of the prediction of the contribution of convective clouds to aerosol wet deposition. Textor et al. (2006) found that the predicted contribution of convective clouds to global and annual mean aerosol wet deposition ranged between 10 and 90 %. Thus, there is no clear consensus on how greatly convective clouds contribute to aerosol removal from the atmosphere. The focus of this study is to examine how the assumptions made in convective cloud schemes can influence predicted aerosol concentrations and wet deposition.

ACPD
12, 1687–1732, 2012

Wet scavenging of aerosols in global models is commonly treated with prescribed scavenging fractions. Global models often assume fixed values to represent the fraction of aerosols that are cloud-droplet-borne and ice-crystal-borne, and susceptible to removal by convective precipitation formation (Liu et al., 2001; Stier et al., 2005; Donner et al., 2011; Fang et al., 2011). The fraction of aerosol mass that is cloud-droplet-borne is typically assumed to be near unity for accumulation and coarse mode aerosols in warm phase convective clouds. However, for aerosol number in the nucleation and Aitken modes, and for both aerosol mass and number in mixed and ice phase clouds, these assumptions about the cloud-droplet-borne and ice-crystal-borne fractions vary considerably between models. Additionally, since clouds often occur at a scale smaller than the typical grid-box size of a global model, the precipitation fraction of the grid box is also parameterized, often as a function of an assumed or parameterized updraft velocity (Liu et al., 2001; Stier et al., 2005). One goal of this study is to explore a more physical link between convective cloud microphysics and aerosol wet scavenging in a global model, and examine the influence of certain convective cloud assumptions on aerosol concentrations.

A key uncertainty related to convective cloud schemes in global models is the treatment of the influence of entrainment and detrainment processes on convective cloud droplet number concentration. The effects related to entrainment have been examined recently (Barahona and Nenes, 2007). Morales et al. (2011) developed an entraining droplet activation parameterization, and found that cloud droplet number concentration in non-precipitating shallow cumulus clouds was over-predicted by 45 % with an adiabatic parameterization that neglected entrainment effects. Considering both the liquid and ice phase, and deeper convective clouds, Fridland et al. (2004) found in a modeling study that allowing aerosols to entrain above cloud base, and act as cloud condensation and ice nuclei, could enhance the number of ice crystals/cloud droplets in upper cloud regions by about an order of magnitude. Recent work has shown that observed ice crystal concentrations can be artificially high as a result of ice crystal shattering on aircraft measurement probes (Korolev et al., 2011). Neverthless, from a modeling

ACPD
12, 1687–1732, 2012

perspective Fridland et al. (2004) did show that assumptions about the activation of aerosols entrained above the cloud base can significantly influence the predicted number of cloud droplets/ice crystals in deep convective clouds. There remains uncertainty about how greatly deep convective clouds can entrain air above cloud base, and still maintain momentum. However, work by Romps and Kuang (2010) suggests that deep convective clouds can be highly diluted and still maintain momentum sufficient to reach the tropopause. Despite these gaps in our knowledge, the representation of entrainment and detrainment rates is fundamental to convective parameterizations (Tiedtke, 1989).

The influence of entrainment on convective cloud droplet number concentration is often treated with empirical corrections to droplet activation schemes such as the Lin and Leaitch (1997) scheme used by Lohmann (2008). One issue with these fixed empirical corrections is that the supersaturation experienced by entrained air parcels may not always evolve in the same manner for all convective clouds depending on the interplay of several factors including the following. (1) How completely does the entrained air parcel mix with the existing cloud? In the case of negligible mixing, there is low droplet surface area in the entrained parcel, and supersaturations could be high enough to activate the entrained aerosols if the entrained parcel accelerates sufficiently. On the other hand if the entrained parcel completely mixes with the existing cloud, the high droplet surface area prohibits further increases in supersaturation such that the entrained aerosols can not activate. The supersaturation in the updraft may actually reduce if the entrained air is drier, leading to droplet evaporation and a reduction of the already existing cloud droplet number. (2) How has rainout influenced the droplet population? In the case of rainout, the droplet surface area is lowered, and an entrained parcel could experience supersaturations required for activation if the parcel accelerates sufficiently. (3) How has detrainment influenced the cloud droplet number? In the case of a reduction in droplet surface area by detrainment, an entrained aerosol parcel could experience the required supersaturations for aerosol activation. (4) How much momentum dilution occurs as a result of entrainment, which limits the generation

ACPD
12, 1687–1732, 2012

of supersaturation? (5) How much is the supersaturation in the updraft reduced as a result of the entrained air being drier than the updraft? Thus, there are complex and potentially opposing effects related to the influence of entrainment and detrainment on the number of cloud droplets/ice crystals in convective clouds.

In this study, we introduce into the ECHAM5-HAM model an explicit representation of the convective cloud-droplet-borne/ice-crystal-borne aerosol mass and number based on the convective cloud microphysics of Lohmann (2008). We consider two limiting related to the convective wet scavenging of entrained aerosols. The first limiting case allows only those aerosols entering at the cloud base to become cloud-droplet-borne/ice-crystal-borne and susceptible to removal by convective precipitation formation. The second limiting case allows aerosols entrained above the cloud base to activate and become cloud-droplet-borne/ice-crystal-borne. We also compare to the standard ECHAM5-HAM model, which does not explicitly treat the cloud-droplet-borne/ice-crystal-borne aerosol fraction as a function of the cloud microphysics, but rather uses prescribed fractions. We examine the sensitivity of aerosol concentrations, burdens and wet deposition between these simulations. The following section gives a model description. Results are summarized in Sect. 3. Section 3.1 examines the effects of these convective cloud schemes on aerosol concentrations. Section 3.2 considers the sensitivity of aerosol wet deposition to the convective cloud assumptions. Section 3.3 compares our simulated results with observations of global aerosol optical depth, wet deposition, and aerosol vertical profiles.

2 Model description and development

The ECHAM5 model is a fifth generation atmospheric general circulation model (GCM) developed at the Max-Planck Institute for Meteorology (Roeckner et al., 2003), and evolved from the model of the European Centre for Medium Range Weather Forecasting (ECMWF). The model solves prognostic equations for vorticity, divergence, temperature and surface pressure using spheric harmonics with triangular truncation. Water

ACPD
12, 1687–1732, 2012

vapor, cloud liquid water and ice are transported using a semi-Lagrangian scheme (Lin and Rood, 1996). Prognostic equations for cloud water and ice follow the two-moment cloud microphysics scheme of Lohmann et al. (2007). The model includes the cirrus scheme of Lohmann and Kärcher (2002). Convective clouds, and convective transport are based on the mass-flux scheme of Tiedtke (1989) with modifications following Nordeng (1994). For this study, we have implemented the two-moment convective cloud microphysics scheme of Lohmann (2008). The solar radiation scheme has 6 spectral bands (Cagnazzo et al., 2007) and the infrared has 16 spectral bands (Mlawer et al., 1997; Morcrette et al., 1998).

Additionally, for this study, the GCM is coupled to the Hamburg Aerosol Model (HAM), which is described in detail in Stier et al. (2005). The aerosols are represented by seven log-normal modes, 4 soluble/internally mixed modes (nucleation – NS, Aitken – KS, accumulation – AS, and coarse – CS) and 3 insoluble modes (Aitken – KI, accumulation – AI, and coarse – CI). The simulated aerosol species are sulfate, black carbon, particulate organic matter, sea salt and dust. The count median radius for each mode is calculated from the aerosol mass and number distributions in each mode. Aerosol mass and number are transferred between the modes by the processes of sulfuric acid condensation, and aerosol coagulation. All results presented in this study are from five year free-running simulations, following a three months spin-up period, using climatological sea surface temperatures and sea ice extent. Aerosol emissions are taken from the AEROCOM database and are representative for the year 2000 (Dentener et al., 2006b). The aerosol emissions and the removal processes of sedimentation, and dry deposition are described in detail in Stier et al. (2005). The below-cloud and stratiform in-cloud scavenging schemes of Croft et al. (2009, 2010) are employed for this study.

2.1 Convective aerosol wet scavenging parameterizations

Here we describe the different convective wet scavenging, and cloud droplet number concentration parameterizations used in this study.

ACPD
12, 1687–1732, 2012

2.1.1 Original convective wet scavenging parameterization

The in-cloud aerosol scavenging parameterization for convective clouds in the standard ECHAM5-HAM model follows Stier et al. (2005). The scavenging of aerosols in convective clouds is coupled to the mass flux scheme of convective tracer transport of Tiedtke (1989). In the convective updrafts, the fraction of aerosol mass and number that are cloud-droplet-borne and ice-crystal-borne are prescribed as a function of the aerosol mode alone for the purposes of the wet removal parameterization. These prescribed fractions, R_i, are given in Table 1. The cloud-droplet-borne and ice-crystal-borne fractions are assumed to be equal for each aerosol mode. The change in the i-th tracer due to convective wet deposition at each model layer is

$$\Delta C_i = C_i^{\mathrm{liq}} R_i E^{\mathrm{liq}} + C_i^{\mathrm{ice}} R_i E^{\mathrm{ice}} \tag{1}$$

where C_i^{liq} and C_i^{ice} are the concentrations of tracer associated with the liquid and ice phase, E^{liq} and E^{ice} are the fraction of liquid and ice water, respectively, that are converted to precipitation. This standard model scheme allows for scavenging in mixed liquid and ice phase clouds since tracer concentrations associated with the liquid and ice phase can co-exist.

For each model layer, a grid box mean deposition flux $\overline{F_i^{\mathrm{dep}}}$ is found

$$\overline{F_i^{\mathrm{dep}}} = \Delta C_i \overline{F^{\mathrm{up}}} \tag{2}$$

where $\overline{F^{\mathrm{up}}}$ is the grid box mean updraft mass flux. The grid box mean tracer tendency is

$$\frac{\overline{\Delta C_i}}{\Delta t} = \overline{F_i^{\mathrm{dep}}} \frac{g}{\Delta p} \tag{3}$$

where g is the acceleration due to gravity and Δp is the model layer thickness in pressure units. The tracers deposition fluxes are integrated from the model top downward.

ACPD
12, 1687–1732, 2012

The mean updraft tracer flux for the i-th tracer is recalculated as

$$\overline{F_i^{\text{up}}} = (C_i - \Delta C_i)\overline{F^{\text{up}}} \tag{4}$$

Finally, the fraction of evaporating precipitation is used to reduce the integrated tracer deposition flux as described in detail in Stier et al. (2005). This scavenging parameterization implicitly allows for aerosols that are entrained into the updraft above the cloud base to become cloud-droplet-borne/ice-crystal-borne and removed by precipitation formation since the aerosol concentrations, C_i, at each layer are adjusted by prescribed entrainment and detrainment rates.

2.1.2 New convective wet scavenging parameterization

The new, more physically detailed parameterization for convective aerosol wet scavenging is linked more closely to the convective cloud microphysics of Lohmann (2008). The convective cloud droplet number concentration (CDNC) following the Lohmann (2008) scheme allows for activation only of those aerosols that enter the cloud at the cloud base layer. The CDNC is transported upwards in the convective updraft. The microphysical conversion rates in the updraft include, autoconversion of cloud droplets to form raindrops, heterogeneous contact and immersion freezing of cloud droplets, aggregation of ice crystals to form snow flakes, and accretion of raindrops with cloud droplets, and accretion of snow flakes with both cloud droplets and ice crystals. The convective cloud cover, b^{conv}, is obtained from the updraft mass flux

$$b^{\text{conv}} = \frac{\overline{F^{\text{up}}}}{\rho \omega_u} \tag{5}$$

where ρ is the air density and ω_u is an assumed vertical velocity ($2\,\text{m}\,\text{s}^{-1}$). The convective cloud microphysics scheme is described in detail in Lohmann (2008).

The activation scheme used throughout this study is the Ghan et al. (1993) scheme. For our study, this scheme is preferred over the Lin and Leaitch (1997) scheme since

ACPD
12, 1687–1732, 2012

the Ghan et al. (1993) scheme does not implicitly account for the effects of entrainment on the number of activated droplets. The number of activated droplets is

$$N_{\mathrm{l,ghan}} = \frac{\omega N_{\mathrm{aer>25\,mn}}}{\omega + \beta N_{\mathrm{aer>25\,nm}}} \tag{6}$$

where $N_{\mathrm{aer>25\,mn}}$ are the number of aerosols larger than 25 nm in radii, β is $0.0034\,\mathrm{cm}^{-4}\,\mathrm{s}^{-1}$, and w is the vertical velocity used by the activation scheme such that

$$\omega = \overline{\omega} + 2\sqrt{\mathrm{CAPE}} + 0.7\sqrt{\mathrm{TKE}}. \tag{7}$$

CAPE is the convective available potential energy, TKE is the turbulent kinetic energy and $\overline{\omega}$ is the large-scale vertical velocity. The contribution to the vertical velocity from CAPE follows elementary parcel theory (Rogers and Yau, 1989). Elementary parcel theory yields that the vertical velocity is proportional to $2\sqrt{\mathrm{CAPE}}$. This is an upper estimate that can be found in convective cores in the absence of entrainment. Lohmann (2008, 2002) further describe the parameterization of vertical velocity for the purposes of the activation scheme.

Our new parameterization of cloud-droplet-borne aerosols begins with a diagnosis of the mass and number of cloud-droplet-borne aerosols for each aerosol mode at the cloud base. The initial number of aerosols that are cloud-droplet-borne is equated to the convective CDNC at the cloud base. This number is apportioned between the aerosol modes, and separate cloud-droplet-borne mass fractions are calculated as described in detail in Croft et al. (2010). The remaining interstitial aerosols can become cloud-droplet-borne or ice-crystal-borne by collision processes. The prescribed collision kernels of Hoose et al. (2008) are used for this study. The aerosol mass and number that are cloud-droplet-borne, ice-crystal-borne and in the interstitial phase for each mode are treated as separate variables in our model in order to calculate the wet removal of the aerosol mass and number for each mode within the context of the convective tracer transport scheme. These auxiliary variables are not passed between

ACPD
12, 1687–1732, 2012

time-steps in our model since the convective clouds collapse after each time-step. As the cloud droplets move up through the model vertical layers due to the updrafts, the cloud-droplet-borne aerosol mass and number are transported upwards, and are modified at each vertical level based on the microphysical conversion rates for freezing and precipitation formation. Aerosols are also released to the interstitial phase by evaporation due to the Bergeron-Findeisen process. Aerosols entrained above the cloud base can enter the cloud droplets and ice crystals by collisions, but not by activation, following the Lohmann (2008) convective cloud microphysics. This scheme allows for mixed liquid and ice phase clouds.

The equation that governs the cloud-droplet-borne aerosol mass as it moves up in the modeled vertical layers for the j-th aerosol mode and for the model level k is

$$m_{j,k,\mathrm{CDCV}} = m_{j,k-1,\mathrm{CDCV}} + \Delta m_{j,k,\mathrm{coll}} - \Delta m_{j,k,\mathrm{frz}} - \Delta m_{j,k,\mathrm{BFP}} - \Delta m_{j,k,\mathrm{auto}} - \Delta m_{j,k,\mathrm{acc}} \quad (8)$$

where $m_{j,k-1,\mathrm{CDCV}}$ is the cloud-droplet-borne aerosol mass in the cloud droplets from the underlying model layer, and the mass change is $\Delta m_{j,k,\mathrm{coll}}$ due to collisions between cloud droplets and interstitial aerosols, $\Delta m_{j,k,\mathrm{frz}}$ due to freezing, $\Delta m_{j,k,\mathrm{BFP}}$ due to evaporation during the Bergeron Findeisen process, and $\Delta m_{j,k,\mathrm{auto}}$ and $\Delta m_{j,k,\mathrm{acc}}$ due to autoconversion and accretion, respectively. Similar processes are considered for the cloud-droplet-borne aerosol number.

The processes that modify the ice-crystal-borne aerosol mass for the j-th mode and for the model level k are

$$m_{j,k,\mathrm{ICCV}} = m_{j,k-1,\mathrm{ICCV}} + \Delta m_{j,k,\mathrm{colli}} + \Delta m_{j,k,\mathrm{frz}} - \Delta m_{j,k,\mathrm{agg}} - \Delta m_{j,k,\mathrm{acc}} \quad (9)$$

where $m_{j,k-1,\mathrm{ICCV}}$ is the ice-crystal-borne aerosol mass from the underlying model layer, and the mass change is $\Delta m_{j,k,\mathrm{colli}}$ due to collisions between ice crystals and interstitial aerosols, $\Delta m_{j,k,\mathrm{frz}}$ due to freezing, and $\Delta m_{j,k,\mathrm{agg}}$ due to aggregation. There is a similar treatment for the aerosol number that is ice-crystal-borne.

The interstitial aerosol mass is

$$m_{j,k,\mathrm{inter}} = m_{j,k-1,\mathrm{inter}} + \Delta m_{j,k,\mathrm{BFP}} - \Delta m_{j,k,\mathrm{coll}} - \Delta m_{j,k,\mathrm{colli}} \quad (10)$$

ACPD
12, 1687–1732, 2012

where $m_{j,k-1,\text{inter}}$ is the interstitial aerosol mass from the underlying model layer. The interstitial aerosol number is treated similarly.

Following this diagnosis of the cloud-droplet-borne and ice-crystal-borne aerosol, the convective wet scavenging parameterization can proceed similarly to that for the standard model, within the context of the convective tracer transport scheme. However, the cloud-droplet-borne and ice-crystal-borne fractions, R_j, are explicitly diagnosed for each mode and each model level, and also separately for the liquid and ice phase. The cloud-droplet-borne aerosol mass fraction is

$$R_{j,k,\text{liq}} = \frac{m_{j,k,\text{CDCV}}}{m_{j,k,\text{CDCV}} + m_{j,k,\text{ICCV}} + m_{j,k,\text{inter}}} \tag{11}$$

and the ice-crystal-borne aerosol mass fraction is

$$R_{j,k,\text{ice}} = \frac{m_{j,k,\text{ICCV}}}{m_{j,k,\text{CDCV}} + m_{j,k,\text{ICCV}} + m_{j,k,\text{inter}}} \tag{12}$$

There is a similar treatment for the aerosol number tracers. The change of the j-th tracer due to convective wet deposition at model level k is

$$\Delta C_{j,k} = C_{j,k}^{\text{liq}} R_{j,k,\text{liq}} E^{\text{liq}} + C_{j,k}^{\text{ice}} R_{j,k,\text{ice}} E^{\text{ice}}. \tag{13}$$

2.1.3 Limiting cases: new convective cloud droplet number concentration parameterization

The convective CDNC parameterization originally developed by Lohmann (2008) did not explicitly account for the possibility of entrained aerosols to become activated above the cloud base, nor the explicit detrainment of the CDNC except at cloud top. For one limiting case, as a lower bound, we keep the original Lohmann (2008) convective cloud number parameterization, which allows cloud droplet activation only at cloud base, and detrainment at cloud top, and similarly we extend this to allow aerosol entrainment into the updraft at cloud base only, and aerosol detrainment only at cloud top. In the second limiting case, as an upper bound of the influence of entrainment and detrainment

ACPD
12, 1687–1732, 2012

on the convective CDNC, we revise the convective CDNC parameterization and allow aerosols to entrain and activate above the cloud base, assuming negligible mixing with the existing updraft. We also allow cloud droplet and aerosol detrainment at all model levels above cloud base. This allows us to investigate the sensitivity of aerosol concentrations and wet removal to different limiting assumptions that could be made by convective cloud schemes. Both limiting cases implement our new calculated convective cloud-droplet-borne and ice-crystal-borne aerosol fractions, which replace the prescribed fractions of Stier et al. (2005).

To implement this second limiting case, we use the model prediction of the number of aerosols that are entrained into the updraft at each vertical level. We assume that 100 % of these aerosols having radii greater than 25 nm can participate in the Ghan et al. (1993) activation scheme, and apply this activation scheme at each model level from the cloud base layer upwards. The number of newly formed cloud droplets is added to the cloud droplet number that is transported up from the underlying model layer. The supersaturation required to activate entrained aerosols could develop if the entrained air parcel accelerates and is exposed to low cloud droplet surface area either because there is negligible mixing with the existing updraft air, or rain-out or dilution has reduced the CDNC. These conditions are more likely representative of precipitating deep convective clouds. The prescribed entrainment rates in our model for shallow, midlevel and penetrative convection are 1×10^{-3}, 1×10^{-4}, and 2×10^{-4} m^{-1}, respectively. Further details about the calculation of entrainment and detrainment rates are in Tiedtke (1989) and Nordeng (1994).

These additional terms due to activation of aerosols entrained above cloud base, and detrainment are used to adjust the convective CDNC and resultant cloud-droplet-borne aerosol mass and number variables,

$$m_{j,k,\mathrm{CDCV}} = m_{j,k-1,\mathrm{CDCV}} + \Delta m_{j,k,\mathrm{act,ent}} + \Delta m_{j,k,\mathrm{coll}} - \Delta m_{j,k,\mathrm{frz}} - \Delta m_{j,k,\mathrm{BFP}} - \Delta m_{j,k,\mathrm{auto}} - \Delta m_{j,k,\mathrm{acc}} - \Delta m_{j,k,\mathrm{det}} \quad (14)$$

where $\Delta m_{j,k,\mathrm{act,ent}}$ is the cloud-droplet-borne mass change due to entrained aerosols

ACPD
12, 1687–1732, 2012

becoming activated and $\Delta m_{j,k,\mathrm{det}}$ is the change due to detrainment of the cloud droplets. There is a similar treatment for aerosol number in the cloud droplets.

2.2 Model simulations

Table 2 summarizes the model simulations that were conducted for this study. Simulation PF_init is the control simulation with the standard ECHAM5-HAM model and with the convective microphysics of Lohmann (2008). There is entrainment and detrainment of aerosols along the convective updraft. The initial convective cloud droplet number concentration (CDNC) is determined based on activation at cloud base, and this CDNC is transported upwards and modified only by freezing, evaporation, rain-out in the updraft, and cloud-top detrainment. For the aerosol wet removal, the fraction of aerosol mass and number that are cloud-droplet-borne and ice-crystal-borne are prescribed fractions (PF), which are given in Table 1 and follow Stier et al. (2005). Simulation CF_init is identical to PF_init except that the Lohmann (2008) convective cloud microphysics is used to determine the calculated fraction (CF) of aerosol number and mass that is either cloud-droplet-borne, or ice-crystal-borne as described in the previous section. Similar to simulation PF_init, there is entrainment and detrainment of aerosols along the convective shaft, the initial convective CDNC is determined by activation of aerosols at the cloud base, with modifications only by freezing, evaporation, rain-out and cloud-top detrainment. Aerosols do not activate above cloud base, but can enter cloud droplets and ice crystals by collisions.

Figure 1 shows a schematic describing the model set-up for the calculated fractions (CF) simulations. The first limiting case simulation is CF_pipe, which is similar to CF_init, except that aerosols are not allowed to entrain above cloud base and aerosols detrain only at cloud top, similar to the cloud droplets in simulation CF_init. We calculate the cloud-droplet-borne and ice-crystal-borne aerosol fractions as described previously. The second limiting simulation is CF_ed. This simulation is similar to simulation CF_init except that the aerosols entrained above the cloud base are allowed to activate and the cloud droplets are also allowed to detrain at all levels above the cloud base,

ACPD
12, 1687–1732, 2012

similar to the aerosols in simulation CF_init. As well, the aerosols are allowed to detrain and entrain above the cloud base at all model levels. The cloud-droplet-borne and ice-crystal-borne aerosol fractions are calculated as described in the previous section based on the convective cloud microphysics.

3 Discussion

3.1 Effects of convective cloud schemes on aerosol concentrations

3.1.1 Effects of explicit calculation of aerosol into convective cloud condensate

We introduce an explicit calculation of the fraction of aerosol in the convective updrafts that is cloud-droplet-borne and ice-crystal-borne, based on the convective cloud microphysics of Lohmann (2008) (simulation CF_init). This replaces the prescribed fractions (Table 1) used for the convective wet scavenging parameterization in the control simulation PF_init.

Figure 2b and c shows the absolute and relative differences between simulation PF_init and CF_init considering the predicted annual, zonal mean vertical profiles of soluble/internally mixed accumulation mode aerosol mass. The soluble/internally mixed accumulation mode mass concentrations are increased by a factor of two in the lower tropical troposphere and by about one order of magnitude in the upper tropical troposphere for simulation CF_init relative to simulation PF_init. This occurs since the aerosol wet removal for the simulation PF_init is more vigorous than for simulation CF_init. For simulation PF_init, aerosols are entrained along the entire updraft shaft and 99 % of accumulation mode aerosols in the updraft are assumed to be cloud-droplet-borne and ice-crystal-borne and susceptible to removal by precipitation formation. On the other hand, for simulation CF_init only those aerosols entering the updraft at the cloud base are allowed to become cloud-droplet-borne and ice-crystal-borne as a result of acting as a cloud droplet nucleus, although aerosols entrained above the cloud base can

ACPD
12, 1687–1732, 2012

enter the cloud droplets and ice crystals by collisions. These assumptions are consistent with the convective microphysics of Lohmann (2008). This limits the aerosol wet removal since aerosols entrained above the cloud base do not activate to form additional cloud droplets. Wet removal budgets are examined in greater detail in Sect. 3.2. In Sect. 3.1.2 we also explore how greatly cloud droplet-aerosol collisions contribute to aerosol removal in our model by comparing simulation CF_init with the limiting case simulation CF_pipe, which does not allow aerosol entrainment above the cloud base.

Table 3 shows the global and annual mean aerosol burdens, lifetimes, and the aerosol optical depth (AOD) for the simulations PF_init and CF_init. Simulation PF_init has lower aerosol burdens, lifetimes and AOD, about a factor of 0.6 relative to simulation CF_init (and lowest amongst all simulations) as a consequence of more vigourous wet scavenging.

3.1.2 Limiting cases: aerosol pipe versus continuous aerosol entrainment/activation and detrainment

The preceding subsection found a strong sensitivity of the predicted aerosol concentrations to the implementation of calculated cloud-droplet-borne fractions based on the convective cloud microphysics of Lohmann (2008) relative to the use of the prescribed fractions of Stier et al. (2005). We now explore the sensitivity of our new wet removal parameterization to limiting assumptions that could be made for the parameterization of the convective CDNC. We focus on assumptions related to the possibility for entrained aerosols to activate above the cloud base. All of the CF simulations use the convective CDNC to calculate the cloud-droplet-borne aerosol fraction in the updraft. So we first examine the sensitivity of the convective CDNC to the assumptions for our two limiting cases.

Figure 3 shows the annual and zonal mean convective (CV) CDNC for the simulation CF_ed, which revises the Lohmann (2008) convective CDNC parameterization to allow activation of aerosols entrained above the cloud base, and also reduces the CDNC due to detrainment from the updraft shaft. The convective CDNC has a maximum at the

ACPD
12, 1687–1732, 2012

Northern Hemisphere mid-latitudes. There is also a secondary maximum in the tropics. The upper right panel of Fig. 3 shows that the CDNC is larger by up to a factor of two in the tropics for simulation CF_ed compared to simulation CF_pipe. Simulation CF_pipe allows the activation of aerosols at cloud base only, similar to simulation CF_init. This assumption strongly influences the tropical CDNC. As will be examined in Sect. 3.2, the tropical convective precipitation is also reduced for simulation CF_ed relative to simulation CF_pipe. Our result is similar to the result of Fridland et al. (2004) who modeled increased cloud hydrometeor concentrations when aerosols above the cloud base were allowed to entrain and activate. The bottom panels of Fig. 3 show the contribution of activated, entrained aerosols to the CV CDNC, and the reduction due to CV CDNC detrainment, both multiplied by the vertical mass flux, for simulation CF_ed. There is a maximum CDNC detrainment for the Northern Hemisphere mid-latitudes where the CDNC has a maximum, and the entrainment effects on the CDNC have a maximum in the tropics where there is a maximum for the mass of soluble internally mixed mode aerosols as shown in Fig. 2.

Figure 2 shows the vertical profiles of annual, zonal mean soluble/internally mixed accumulation mode mass concentrations for the limiting case simulation CF_ed, and also the absolute and relative differences between all four simulations. The accumulation mode mass concentrations have a maximum in the tropics, north of the equator due to the combination of biomass burning, and dust emissions (panel a). The mass concentrations are increased near this maximum for all simulations relative to the simulation PF_init, which has the most vigorous aerosol wet removal by convective precipitation (wet deposition budgets are in the following subsection). The most pronounced absolute difference between the two limiting cases is in the tropics (panel h). Simulation CF_ed has lower accumulation mode concentrations in the tropical mid-troposphere by about 50 % relative to CF_pipe (panel i) since the aerosol wet removal by convective precipitation is more vigorous when aerosols entrained above cloud base are allowed to activate and become susceptible to removal by convective precipitation formation. This effect is greatest in the tropics where convective precipitation rates

ACPD
12, 1687–1732, 2012

are the largest. Simulation CF_pipe is most similar to simulation CF_init since both of these simulations allow aerosol activation to form cloud droplets in only the cloud base layer. The upper tropospheric concentrations differ about one order of magnitude for simulations CF_pipe and CF_init relative to the standard model simulation PF_init. Simulation CF_ed is closest to the standard model simulation PF_init, but has greater concentrations by about a factor of two in the upper troposphere.

Table 3 shows the global and annual mean aerosol burdens, lifetimes, and the aerosol optical depth (AOD) for these two limiting cases, in addition to those for the PF_init and CF_init simulations. Large differences exist between the two limiting cases. Burdens, lifetimes and aerosol optical depth are about 30 % lower for the simulation CF_ed as compared to CF_pipe. Thus, the net influence of allowing aerosols entrained above the cloud base to activate in the simulation CF_ed yields more vigourous aerosol wet removal in the annual and global mean relative to the limiting case simulation CF_pipe, which allows only aerosols entering the updraft at the cloud base layer to be susceptible to removal by precipitation formation. The aerosol lifetimes are similar between the CF_init and CF_pipe. This shows that collision processes above cloud base make a limited contribution to the uptake of aerosols into the cloud droplets and ice crystals in our model. Allowing cloud droplet activation above cloud base is a strong controlling factor in our model, as is demonstrated by examining the aerosol burdens and lifetimes for simulation CF_ed relative to both CF_init and CF_pipe. Simulation PF_init is most similar to simulation CF_ed since PF_init implicitly assumes that 99 % of soluble accumulation and coarse mode aerosols entrained above the cloud base will become cloud-droplet-borne/ice-crystal-borne and susceptible to removal by precipitation formation. However, burdens, lifetimes and AOD are about 25 % larger for simulation CF_ed relative to simulation PF_init. This can be partly attributed to less aerosol removal in the mixed liquid and ice phase clouds with temperatures between 238 and 273 K as will be examined in further detail in the following section.

ACPD
12, 1687–1732, 2012

3.2 Sensitivity of wet deposition to convective assumptions

Figure 4 shows the annual and global mean aerosol wet deposition attributed to convective precipitation relative to the total wet deposition (including both stratiform and convective precipitation), and also relative to the total aerosol deposition. Particulate organic matter is the aerosol species that has the most wet removal attributed to scavenging in convective clouds relative to the total wet deposition (about 20 and 25 % for simulations CF_pipe and CF_ed, respectively). Convective wet scavenging also makes the greatest contribution to total aerosol deposition for organic matter, followed by black carbon (about 25 and 20 %, respectively for simulation CF_ed). These species have the greatest emissions in regions of high convective precipitation, and do not have fast dry deposition and sedimentation rates like dust or sea salt. Thus, the parameterization of convective wet scavenging is particularly relevant for the carbonaceous aerosols. For the carbonaceous aerosols and sulfate, the fractional contribution of convective wet scavenging to total removal is 20 % greater for the simulation CF_ed as compared to CF_pipe and this contributes to the 30 % shorter aerosol lifetimes as shown in Table 3. All of our results for the fractional contribution of convective wet deposition to total wet deposition are in the lower end of the 10–90 % range of Textor et al. (2006), and similar to the results of Fang et al. (2011) with the AM3 global model. The fractional contribution of convective wet deposition to total wet deposition varies with species and is greatest for simulation PF_init (between 20 to 35 %), and is least for simulation CF_pipe (between 10 and 20 %). Thus, differences in the convective cloud assumptions related to the activation of aerosols entrained above cloud base, as for our simulations CF_pipe and CF_ed, can not entirely account for the 10–90 % range of Textor et al. (2006). Other factors, such as the convective transport parameterization, can contribute to this discrepancy as was found by Tost et al. (2010).

Figures 5 and 6 show the annual mean geographic distribution of convective wet deposition for the five aerosol species for the simulation CF_ed and also the absolute difference compared with the other limiting case simulation CF_pipe. The convective

ACPD
12, 1687–1732, 2012

wet deposition is increased by up to a factor of two in the tropics for all aerosol species except sea salt for the simulation CF_ed as compared to CF_pipe. This occurs since aerosols entrained above cloud base are allowed to become cloud-droplet-borne and susceptible to removal by precipitation formation for simulation CF_ed, unlike for simulation CF_pipe. Interestingly, this increase in wet deposition occurs despite the concurrent decrease in the convective precipitation rate for several tropical locations such as in the tropical Indo-Asian and South American areas (bottom right panel of Fig. 6). Sea salt has decreased wet deposition for simulation CF_ed relative to CF_pipe, by up to a factor of two. For many geographic regions this is associated with a reduction in the precipitation rate. The bottom panels of Fig. 6 show the geographic distribution of convective precipitation and the absolute difference between simulations CF_ed and CF_pipe. We note that the regions of convective wet deposition maxima are generally coincident with the precipitation maxima. The global and annual mean precipitation was 1.7 and 1.4 m yr^{-1} for the simulations CF_pipe and CF_ed, respectively. This precipitation change is associated with the changes to the convective CDNC parameterization between these two simulations.

Tables 4–8 summarize the annual mean deposition budgets for the five aerosol species. The different convective cloud assumptions between the two limiting cases (CF_pipe and CF_ed) strongly influence the convective wet deposition budgets. The convective wet deposition attributed to warm and mixed phase clouds is greater by a factor of about 3 for sulfate, carbonaceous aerosols and dust for the CF_ed compared to the CF_pipe simulation. As a result, the scavenging by ice phase clouds is reduced by more than one order of magnitude for simulation CF_ed relative to CF_pipe. While the warm phase scavenging is similar between CF_ed and PF_init, the mixed phase scavenging is lower for all CF simulations relative to simulation PF_init (by about one half to one third for simulation CF_ed). Thus, the wet removal based on prescribed fractions as a function of aerosol mode alone, and applied across the entire cloud temperature range, is not consistent with the wet removal based on cloud-droplet-borne/ice-crystal-borne fractions calculated from the convective cloud microphysics. Our results point

ACPD
12, 1687–1732, 2012

to the importance of the convective cloud scheme assumptions in the prediction of the wet removal of aerosols attributed to convective precipitation.

Convective below-cloud scavenging is not included in Tables 4–8 since for all simulations the parameterization of this process gives a negligible result relative to that for stratiform clouds. In our model convective below-cloud scavenging can only occur in grid boxes that are completely cloud-free, which limits the contribution from this process. This process was not revised for this study, but should be examined in future work.

3.3 Comparison with observations

Figure 7 shows the annual mean geographic distribution of aerosol optical depth (AOD) from the MODIS/MISR/AERONET data set of van Donkelaar et al. (2010). The AOD maxima are associated with dust emissions from Africa, and anthropogenic pollution sources from Asia and India. The simulation CF_ed has the closest agreement with the MODIS/MISR/AERONET retrieval. The convective scavenging for simulation CF_pipe was less vigorous and this leads to an over-estimate of tropical AOD by up to a factor of three, particularly over the tropical oceans, and more remote to sources. Simulation PF_init has the most vigorous convective wet scavenging, but this underestimates the AOD, particularly associated with the African dust maximum by about 50 %.

Figure 8 shows a scatter plot of observed and modeled sulfate wet deposition. The observations are from the global dataset of Dentener et al. (2006a), but restricted to latitudes between 30° S and 30° N. All simulations are reasonable and have similar scatter with about two-thirds of the modeled deposition being within a factor of two of the observations. The slope parameter shows that the model underestimates sulfate wet deposition in the tropical regions, which may indicate missing sources since sulfate production in convective clouds is not included in our model. The correlation coefficient is lowest for the PF_init simulation (0.55) and only slightly improved for all CF simulations (0.57–0.58).

ACPD
12, 1687–1732, 2012

Comparisons with aircraft observations of black carbon at tropical latitudes (Koch et al., 2009, 2010) are shown in Fig. 9. The agreement between the observations and the model is best and similar for the simulation PF_init and CF_ed, except that PF_init underestimates the concentrations in the upper troposphere by a factor of 2 relative to the observations. The agreement with upper tropospheric observations is closer for CF_ed. The black carbon concentrations in the upper troposphere differ by up to one order of magnitude between the two limiting cases (CF_pipe and CF_ed), and also between the standard model simulation PF_init and the calculated fractions simulation CF_init. Thus convective clouds assumptions, particularly about how aerosols entrain and become cloud-droplet-borne above cloud base are shown to strongly influence predicted aerosol concentrations.

4 Conclusions

We examined the sensitivity of aerosol concentrations, burdens, lifetimes and wet deposition to limiting assumptions made by convective cloud schemes in a global climate model. To facilitate this study, we coupled the two-moment convective cloud microphysics of Lohmann (2008) to the aerosol wet scavenging parameterizations of the ECHAM5-HAM global climate model. Similar to many global models, the standard ECHAM5-HAM model assumes prescribed fractions of the aerosol mass and number are cloud-droplet-borne and ice-crystal-borne, and thus susceptible to wet removal by convective precipitation formation. We introduced into the ECHAM5-HAM model an explicit representation of the uptake of aerosol mass and number into convective cloud droplets and ice crystals by the processes of activation, collisions, freezing and evaporation to provide a closer coupling with the convective microphysics scheme of Lohmann (2008). This allowed an explicit calculation of the fraction of aerosol mass and number that was cloud-droplet-borne and ice-crystal-borne, and susceptible to convective wet deposition. The standard model had more vigorous convective wet removal, and the annual and global mean aerosol burdens were about 0.6 of those

ACPD
12, 1687–1732, 2012

with the revised convective wet deposition parameterization. Aerosol concentrations in the upper troposphere differed by up to one order of magnitude. The wet removal attributed to scavenging in convective clouds between temperatures of 238 and 273 K where the liquid and ice phase could co-exist was reduced by a factor of two to five with the revised convective wet deposition parameterization, suggesting that implementation of a single prescribed fraction as a function of aerosol mode, applied for the entire temperature range (as for the standard model), was not consistent with the convective microphysics.

The parameterization of the influences of entrainment and detrainment on convective cloud droplet number number concentration (CDNC) in global models is associated with considerable uncertainty. As a result, two limiting cases were considered in this study. In the first case, the convective updraft was considered to behave like an isolated pipe for aerosols and cloud droplets; aerosol activation was allowed only at the cloud base layer and detrainment of aerosols and cloud droplets/ice crystals occurred only at the cloud top. In the second limiting case, aerosols were allowed to entrain and detrain along the updraft, and the entrained aerosols could activate above the cloud base layer, and the CDNC could detrain the along the updraft. Allowing activation of aerosols entrained above cloud base enhanced by a factor of two the annual and zonal mean convective CDNC in the tropics. Convective wet scavenging was more vigorous, which lowered by 30 % the annual and global mean aerosol burdens and lifetimes. Aerosol concentrations differed by up to one order of magnitude in the upper troposphere between the two limiting cases. Closest agreement with observations of the geographic distribution of the annual mean aerosol optical depth, particularly in the tropics, was found for the convective cloud scheme that allowed aerosols entrained above cloud base to activate and become cloud-droplet-borne/ice-crystal-borne. The sensitivity of aerosol concentrations to these convective cloud assumptions motivates the need for on-going observations coupled with modeling studies to better elucidate the role of convective precipitation scavenging of aerosols in the global climate system.

ACPD
12, 1687–1732, 2012

The results of this study point to the importance of ongoing work to understand the kinematics of convective clouds, and convective entrainment and detrainment rates. Our results suggest that parameterizations of convective CDNC for global models should account for the possibility of aerosols entrained in the updrafts to become activated. This is particularly relevant for the tropics with intense convective precipitation. Due to the possibility of other model errors, we can not conclusively state what are the best entrainment and detrainment assumptions based on this work. However, we have shown a strong sensitivity of aerosol concentrations (differences of one order of magnitude in the upper troposphere between our simulations) depending on the convective cloud assumptions related to entrained aerosols and their possibility to become cloud-droplet-borne/ice-crystal-borne. Scavenging parameterizations should be developed that account for the possibility of aerosols that are entrained above cloud base to become cloud-droplet-borne/ice-crystal-borne, and thus susceptible to wet removal, although concurrently detrainment processes must also be considered. In order to improve convective wet scavenging parameterizations in global models, ongoing field work and case studies are needed with an emphasis on examining how readily aerosols are entrained and become cloud-droplet-borne/ice-crystal-borne in the convective updrafts. These measurements must involve many varieties of convective cloud conditions. Ultimately, improvements in convective cloud microphysics coupled with more physical wet scavenging parameterizations will improve the prediction of three-dimensional aerosol distributions in our global models and help to resolve the ongoing uncertainty related to how convective clouds contribute to removing particulate matter from the atmosphere.

Acknowledgements. We thank Sylvaine Ferrachat for her technical assistance and Aaron van Donkelaar for providing the MODIS/MISR/AERONET AOD compilation data set. We thank D. Koch, and the following groups associated with providing aircraft data: NOAA at UC Boulder (David Fahey), University of Tokyo (Y. Kondo), and University of Hawaii (T. Clarke). We are grateful to the National Science and Engineering Research Council of Canada (NSERC), the Killam Trusts Foundation of Canada, and the Atlantic Computational Excellence Network (ACE-Net) for financial support. Thanks also to CSCS for computing time.

ACPD
12, 1687–1732, 2012

References

Ackerman, A. S., Toon, O. B., Stevens, D. E., Heymsfield, A. J., Ramanathan, V., and Welton, E. J.: Reduction in tropical cloudiness by soot, Science, 288, 1042–1047, doi:10.1126/science.288.5468.1042, 2000. 1689

Barahona, D. and Nenes, A.: Parameterization of cloud droplet formation in large-scale models: Including effects of entrainment, J. Geophys. Res., 112, D16206, doi:10.1029/2007JD008473, 2007. 1690

Cagnazzo, C., Manzini, E., Giorgetta, M. A., Forster, P. M. De F., and Morcrette, J. J.: Impact of an improved shortwave radiation scheme in the MAECHAM5 General Circulation Model, Atmos. Chem. Phys., 7, 2503–2515, doi:10.5194/acp-7-2503-2007, 2007. 1693

Charlson, R. J., Schwartz, S. E., Hales, J. M., Cess, R. D., Coakley, J. A., Hansen, J. E., and Hofmann, D. J.: Climate forcing by anthropogenic aerosols., J. Geophys. Res., 255, 423–430, 1992. 1689

Croft, B., Lohmann, U., Martin, R. V., Stier, P., Wurzler, S., Feichter, J., Posselt, R., and Ferrachat, S.: Aerosol size-dependent below-cloud scavenging by rain and snow in the ECHAM5-HAM, Atmos. Chem. Phys., 9, 4653–4675, doi:10.5194/acp-9-4653-2009, 2009. 1693

Croft, B., Lohmann, U., Martin, R. V., Stier, P., Wurzler, S., Feichter, J., Hoose, C., Heikkilä, U., van Donkelaar, A., and Ferrachat, S.: Influences of in-cloud aerosol scavenging parameterizations on aerosol concentrations and wet deposition in ECHAM5-HAM, Atmos. Chem. Phys., 10, 1511–1543, doi:10.5194/acp-10-1511-2010, 2010. 1693, 1696

Dentener, F., Drevet, J., Lamarque, J. F., Bey, I., Eickhout, B., Fiore, A. M., Haiglustaine, D., Horowitz, L. W., Krol, M., Lawrence, U. C., Galy-Lacaux, C., Rast, S., Shindell, D., Stevenson, D., Noije, T. V., Atherton, C., Bell, N., Bergman, D., Butler, T., Cofala, J., Colins, B., Doherty, R., Ellingsen, K., Galloway, J., Gauss, M., Montanaro, V., Müller, J. F., Pitari, G., Rodriguez, J., Sanderson, M., Solomon, F., Strahan, S., Schultz, M., Sudo, K., Szopa, S., and Wild, O.: Nitrogen and sulfur deposition on regional and global scales: A multimodel evaluation, Global Biogeochem. Cy., 20, GB4003,doi:10.1029/2005GB002672, 2006a. 1707, 1731

Dentener, F., Kinne, S., Bond, T., Boucher, O., Cofala, J., Generoso, S., Ginoux, P., Gong, S., Hoelzemann, J. J., Ito, A., Marelli, L., Penner, J. E., Putaud, J.-P., Textor, C., Schulz, M., van der Werf, G. R., and Wilson, J.: Emissions of primary aerosol and precursor gases in the years 2000 and 1750 prescribed data-sets for AeroCom, Atmos. Chem. Phys., 6, 4321–4344,

ACPD
12, 1687–1732, 2012

doi:10.5194/acp-6-4321-2006, 2006b. 1693
Dockery, D. W., Pope III, C. A., Xu, X., Spengler, J. D., Ware, J. H., Fay, M. E., Ferris, B. G. ., and Speizer, F. E.: An association between air pollution and mortality in six U.S. Cities, N. Engl. J. Med., 329, 1753–1759, 1993. 1689
Donner, L. J., Wyman, B. L., Hemler, R. S., Horowitz, L. W., Ming, Y., Zhoa, M., Golaz, J.-C., Ginoux, P., Lin, S.-J., Schwarkopf, M. D., Austin, J., Alaka, G., Cooke, W. F., Delworth, T. L., Freidenreich, S. M., Gordon, C. T., Griffies, S. M., Held, I. M., Hurlin, W. J., Klein, S. A., Knutson, T. R., Langenhorst, A. R., Lee, H.-C., Lin, Y., Magi, B. I., Malyshev, S. L., Milly, P. C. D., Naik, V., Nath, M. J., Pincus, R., Ploshay, J. J., Ramaswamy, V., Seman, C. J., Shevliakova, E., Sirutis, J. J., Stern, W. F., Stouffer, R. J., Stouffer, R. J., Wilson, R. J., Winton, M., Wittenberg, A. T., and Zeng, F.: The dynamical core, physical parameterizations, and basic simulation characteristics of the atmospheric component AM3 of the GFDL Global Coupled Model CM3, J. Climate, 24, 3484–3519, 2011. 1690
Engström, A., Ekman, A. M. L., Krejci, R., Ström, J., de Reus, M., and Wang, C.: Observational and modelling evidence of tropical deep convective clouds as a source of mid-tropospheric accumulation mode aerosols, Geophys. Res. Lett., 35, L23813, doi:10.1029/2008GL035817, 2008. 1689
Fang, Y., Fiore, A. M., Horowitz, L. W., Gnanadesikan, A., Held, I., Chen, G., Vecchi, G., and Levy, H.: The impacts of changing transport and precipitation on pollutant distributions in a future climate, J. Geophys. Res., 116, D18303, doi:10.1029/2011JD015642, 2011. 1690, 1705
Fridland, A., Ackermann, A., Jensen, E., and Stevens, D.: Evidence for the predominance of mid-tropospheric aerosols as subtropical anvil nuclei, Science, 304, 718–722, 2004. 1690, 1691, 1703
Ghan, S. J., Chuang, C. C., and Penner, J. E.: A parameterization of cloud droplet nucleation. Part I: Single aerosol type, Atmos. Res., 30, 198–221, 1993. 1695, 1696, 1699
Hansen, J., Sato, M., and Ruedy, R.: Radiative forcing and climate response, J. Geophys. Res., 102, 6831–6864, doi:10.1029/96JD03436, 1997. 1689
Hoose, C., Lohmann, U., Bennartz, R., Croft, B., and Lesins, G.: Global simulations of aerosol processing in clouds, Atmos. Chem. Phys., 8, 6939–6963, doi:10.5194/acp-8-6939-2008, 2008. 1696
Koch, D., Schulz, M., Kinne, S., McNaughton, C., Spackman, J. R., Balkanski, Y., Bauer, S., Berntsen, T., Bond, T. C., Boucher, O., Chin, M., Clarke, A., De Luca, N., Dentener, F., Diehl,

ACPD
12, 1687–1732, 2012

T., Dubovik, O., Easter, R., Fahey, D. W., Feichter, J., Fillmore, D., Freitag, S., Ghan, S., Ginoux, P., Gong, S., Horowitz, L., Iversen, T., Kirkevåg, A., Klimont, Z., Kondo, Y., Krol, M., Liu, X., Miller, R., Montanaro, V., Moteki, N., Myhre, G., Penner, J. E., Perlwitz, J., Pitari, G., Reddy, S., Sahu, L., Sakamoto, H., Schuster, G., Schwarz, J. P., Seland, Ø., Stier, P., Takegawa, N., Takemura, T., Textor, C., van Aardenne, J. A., and Zhao, Y.: Evaluation of black carbon estimations in global aerosol models, Atmos. Chem. Phys., 9, 9001–9026, doi:10.5194/acp-9-9001-2009, 2009. 1708, 1732

Koch, D., Schulz, M., Kinne, S., McNaughton, C., Spackman, J. R., Balkanski, Y., Bauer, S., Berntsen, T., Bond, T. C., Boucher, O., Chin, M., Clarke, A., De Luca, N., Dentener, F., Diehl, T., Dubovik, O., Easter, R., Fahey, D. W., Feichter, J., Fillmore, D., Freitag, S., Ghan, S., Ginoux, P., Gong, S., Horowitz, L., Iversen, T., Kirkevåg, A., Klimont, Z., Kondo, Y., Krol, M., Liu, X., Miller, R., Montanaro, V., Moteki, N., Myhre, G., Penner, J. E., Perlwitz, J., Pitari, G., Reddy, S., Sahu, L., Sakamoto, H., Schuster, G., Schwarz, J. P., Seland, Ø., Stier, P., Takegawa, N., Takemura, T., Textor, C., van Aardenne, J. A., and Zhao, Y.: Corrigendum to "Evaluation of black carbon estimations in global aerosol models" published in Atmos. Chem. Phys., 9, 9001–9026, 2009, Atmos. Chem. Phys., 10, 79–81, doi:10.5194/acp-10-79-2010, 2010. 1708, 1732

Korolev, A. V., Emery, E. F., Strapp, J. W., Cober, S. G., Isaac, G. A., Wasey, M., and Marcotte, D.: Small ice particles in tropospheric clouds: Fact or artifact, B. Am. Meteorol. Soc., 92, 967–973, 2011. 1690

Lin, H. and Leaitch, W. R.: Development of an in-cloud aerosol activation parameterization for climate modelling, in: Proceedings of the WMO Workshop on Measurement of Cloud Properties for Forecasts of Weather, Air Quality and Climate, World Meteorol. Organ., Geneva, 328–335, 1997. 1691, 1695

Lin, S. J. and Rood, R. B.: Multidimensional flux form semi-Lagrangian transport, Mon. Weather Rev., 124, 2046–2068, 1996. 1693

Liu, H., Jacob, D. J., Bey, I., and Yantosca, R. M.: Constraints from ^{210}Pb and ^{7}Be on wet deposition and transport in a global three-dimensional chemical tracer model driven by assimilated meteorolgical fields, J. Geophys. Res., 106, 12109–12128, 2001. 1690

Lohmann, U.: A glaciation indirect effect caused by soot aerosols, Geophys. Res. Lett., 29, 1052, doi:10.1029/2001GL014357, 2002. 1696

Lohmann, U.: Global anthropogenic aerosol effects on convective clouds in ECHAM5-HAM, Atmos. Chem. Phys., 8, 2115–2131, doi:10.5194/acp-8-2115-2008, 2008. 1689, 1691, 1692,

ACPD
12, 1687–1732, 2012

1693, 1695, 1696, 1697, 1698, 1700, 1701, 1702, 1708, 1717, 1724
Lohmann, U. and Kärcher, B.: First interactive simulations of cirrus clouds formed by homogeneous freezing in the ECHAM general circulation model, J. Geophys. Res., 107, 4105, doi:10.1029/2001JD000767, 2002. 1693
Lohmann, U., Stier, P., Hoose, C., Ferrachat, S., Kloster, S., Roeckner, E., and Zhang, J.: Cloud microphysics and aerosol indirect effects in the global climate model ECHAM5-HAM, Atmos. Chem. Phys., 7, 3425–3446, doi:10.5194/acp-7-3425-2007, 2007. 1693
Menon, S. and Rotstayn, L.: The radiative influence of aerosol effects on liquid-phase cumulus and stratiform clouds based on sensitivity studies with two climate models, Clim. Dynam., 27, 345–356, 2006. 1689
Mlawer, E. J., Taubman, S. J., Brown, P. D., Iacono, M. J., and Clough, S. A.: Radiative transfer for inhomogeneous atmosphere: RRTM, a validated correlated-k model for the longwave, J. Geophys. Res., 102, 16663–16682, 1997. 1693
Morales, R., Nenes, A., Jonsson, J., Flagan, R. C., and Seinfeld, J. H.: Evaluation of an entraining droplet activation parameterization using in situ cloud data, J. Geophys. Res., 116, D15205, doi10.1029/2010JD015324, 2011. 1689, 1690
Morcrette, J.-J., Clough, S. A., Mlawer, E. J., and Iacono, M. J.: Impact of a validated radiative transfer scheme, RRTM, on the ECMWF model climate and 10-day forecasts, ECMWF, Reading, UK, technical memorandum 252 edn., 1998. 1693
Nober, F. J., Graf, H.-F., and Rosenfeld, D.: Sensitivity of the global circulation to the suppression of precipitation by anthropogenic aerosols, Global Planet. Change, 37, 57–80, 2003. 1689
Nordeng, T. E.: Extended versions of the convective parameterization scheme at ECWMF and their impact on the mean and transient activity of the model in the tropics, ECMWF, Reading, UK, technical memorandum 206 edn., 1994. 1693, 1699
Randall, D., Khairoutdinov, M., Arakawa, A., and Grabowski, W.: Breaking the cloud parameterization deadlock, B. Am. Meteorol. Soc., 84, 1547–1564, 2003. 1689
Roeckner, E., Baeuml, G., Bonventura, L., Brokopf, R., Esch, M., Giorgetta, M., Hagemann, S., Kirchner, I., Kornblueh, L., Manzini, E., Rhodin, A., Schlese, U., Schulzweida, U., and Tompkins, A.: The atmospheric general circulation model ECHAM5. Part I: Model description, Report 349, Max Planck Institute for Meteorology, Hamburg, Germany, available at: http://www.mpimet.mpg.de, 2003. 1692
Rogers, R. R. and Yau, M. K.: A short course in cloud physics, Butterworth-Heinemann Pub.,

ACPD
12, 1687–1732, 2012

1989. 1696
Romps, D. M. and Kuang, Z.: Do undiluted convective plumes exist in the upper tropical troposphere?, J. Atmos. Sci., 67, 468–484, doi:10.1175/2009JAS3184.1, 2010. 1691
Stier, P., Feichter, J., Kinne, S., Kloster, S., Vignati, E., Wilson, J., Ganzeveld, L., Tegen, I., Werner, M., Balkanski, Y., Schulz, M., Boucher, O., Minikin, A., and Petzold, A.: The aerosol-climate model ECHAM5-HAM, Atmos. Chem. Phys., 5, 1125–1156, doi:10.5194/acp-5-1125-2005, 2005. 1690, 1693, 1694, 1695, 1699, 1700, 1702, 1717, 1724
Textor, C., Schulz, M., Guibert, S., Kinne, S., Balkanski, Y., Bauer, S., Berntsen, T., Berglen, T., Boucher, O., Chin, M., Dentener, F., Diehl, T., Easter, R., Feichter, H., Fillmore, D., Ghan, S., Ginoux, P., Gong, S., Grini, A., Hendricks, J., Horowitz, L., Huang, P., Isaksen, I., Iversen, I., Kloster, S., Koch, D., Kirkevåg, A., Kristjansson, J. E., Krol, M., Lauer, A., Lamarque, J. F., Liu, X., Montanaro, V., Myhre, G., Penner, J., Pitari, G., Reddy, S., Seland, Ø., Stier, P., Takemura, T., and Tie, X.: Analysis and quantification of the diversities of aerosol life cycles within AeroCom, Atmos. Chem. Phys., 6, 1777–1813, doi:10.5194/acp-6-1777-2006, 2006. 1689, 1705
Tiedtke, M.: A comprehensive mass flux scheme for cumulus parameterization in large scale model, Mon. Weather Rev., 117, 1779–1800, 1989. 1691, 1693, 1694, 1699
Tost, H., Lawrence, M. G., Brühl, C., Jöckel, P., The GABRIEL Team, and The SCOUT-O3-DARWIN/ACTIVE Team: Uncertainties in atmospheric chemistry modelling due to convection parameterisations and subsequent scavenging, Atmos. Chem. Phys., 10, 1931–1951, doi:10.5194/acp-10-1931-2010, 2010. 1689, 1705
Twomey, S.: Aerosol, clouds, and radiation, Atmos. Environ., 25A, 2435–2442, 1991. 1689
van Donkelaar, A., Martin, R. V., Brauer, M., Kahn, R., Levy, R., Verduzco, C., and Villeneuve, P.: Global estimates of exposure to fine particulate matter concentrations from satellite-based aerosol optical depth, Environ. Health Persp., 118, 847–855, doi:10.1289/ehp.0901623, 2010. 1689, 1707, 1730

ACPD
12, 1687–1732, 2012

Table 1. Prescribed cloud-droplet-borne fractions as a function of aerosol mode used for the simulation PF_init. The same fractions are used for ice-crystal-borne fractions.

	Soluble/Internally Mixed	Insoluble/Externally Mixed
Nucleation Mode	0.2	
Aitken Mode	0.6	0.2
Accumulation Mode	0.99	0.4
Coarse Mode	0.99	0.4

ACPD
12, 1687–1732, 2012

Table 2. The simulations presented in this study are summarized in this table. Figure 1 shows a schematic of these simulations.

Simulation	Description
PF_init	PF: prescribed cloud-droplet-borne/ice-crystal-borne aerosol fractions of Stier et al. (2005) used for convective wet scavenging, init: following initial (i.e. unmodified) assumptions of the standard ECHAM5-HAM, aerosols entrain and detrain in convective updrafts, convective cloud droplet number concentration (CDNC) based on activation only at cloud base, and CDNC not reduced by detrainment in updrafts, following the Lohmann (2008) cloud microphysics. A control simulation with the standard ECHAM5-HAM model
CF_init	CF: calculated cloud-droplet-borne/ice-crystal-borne aerosol fractions based on convective cloud microphysical processes of Lohmann (2008) used for convective wet scavenging, replacing the prescribed fractions of Stier et al. (2005), init: following initial (i.e. unmodified) assumptions of the standard ECHAM5-HAM as described above for PF_init
CF_pipe	Limiting case 1: CF: calculated cloud-droplet-borne/ice-crystal-borne aerosol fractions as described for CF_init, pipe: updraft is like a pipe for the aerosols, i.e. no entrainment of aerosols in the updraft above cloud base, detrainment only at cloud top, which is similar to the treatment of the convective CDNC following the cloud microphysics of Lohmann (2008)
CF_ed	Limiting case 2: CF: calculated cloud-droplet-borne/ice-crystal-borne aerosol fractions as described for CF_init, ed: entrainment and detrainment explicitly influence the convective CDNC, the Lohmann (2008) convective CDNC parameterization is modified to allow activation of aerosols entrained above cloud base, and CDNC reduced by detrainment at all updraft levels

ACPD
12, 1687–1732, 2012

Table 3. Global and annual mean aerosol burdens (Tg, except Tg S for sulfate) and lifetimes (days) in brackets after the burdens, and aerosol optical depth (AOD) for the four simulations presented in Table 2. The five aerosol species are sulfate (SO4), black carbon (BC), particulate organic matter (POM), dust (DU), and sea salt (SS).

	PF_init	CF_init	CF_pipe	CF_ed
SO_4	0.759 (3.9)	1.22 (6.3)	1.20 (6.2)	0.831 (4.3)
BC	0.119 (5.6)	0.186 (8.8)	0.207 (9.8)	0.146 (6.9)
POM	1.06 (5.9)	1.74 (9.6)	1.93 (10.7)	1.33 (7.3)
DU	6.44 (4.1)	9.95 (5.7)	9.48 (5.3)	8.94 (4.8)
SS	9.12 (0.54)	15.7 (0.93)	14.9 (0.88)	13.9 (0.81)
AOD	0.112	0.176	0.171	0.146

ACPD
12, 1687–1732, 2012

Table 4. Deposition budgets for sulfate (Tg S yr^{-1}) for the four simulations presented in Table 2. Warm refers to cloud temperatures warmer than 273 K, mixed refers to temperatures between 273 and 238 K, and ice refers to temperatures below 238 K. ICS: In-Cloud Scavenging, BCS: Below-Cloud Scavenging, Sed and Dry Dep: Sedimentation and Dry Deposition.

Sulfate	PF_init	CF_init	CF_pipe	CF_ed
Convective ICS				
Warm	9.73	6.88	5.65	8.60
Mixed	4.12	0.57	0.76	1.54
Ice	0.02	0.0004	0.0004	0.0006
Stratiform ICS				
Warm	27.8	29.9	30.6	31.0
Mixed	11.5	14.3	11.9	13.0
Ice	0.75	1.73	1.56	1.00
Stratiform BCS	13.0	13.6	13.9	11.8
Sed and Dry Dep	4.48	4.19	4.13	4.00

ACPD
12, 1687–1732, 2012

Table 5. Deposition budgets for black carbon ($Tg\,yr^{-1}$) for the four simulations presented in Table 2. Warm refers to cloud temperatures warmer than 273 K, mixed refers to temperatures between 273 and 238 K, and ice refers to temperatures below 238 K. ICS: In-Cloud Scavenging, BCS: Below-Cloud Scavenging, Sed and Dry Dep: Sedimentation and Dry Deposition.

Black Carbon	PF_init	CF_init	CF_pipe	CF_ed
Convective ICS				
Warm	1.23	1.04	0.93	1.12
Mixed	0.76	0.12	0.16	0.30
Ice	0.003	0.0002	0.0002	0.0002
Stratiform ICS				
Warm	2.52	2.86	2.97	3.01
Mixed	0.85	1.29	1.25	1.14
Ice	0.07	0.23	0.23	0.14
Stratiform BCS	1.37	1.41	1.43	1.27
Sed and Dry Dep	1.00	0.84	0.82	0.82

ACPD
12, 1687–1732, 2012

Table 6. Deposition budgets for particulate organic matter ($Tg\,yr^{-1}$) for the four simulations presented in Table 2. Warm refers to cloud temperatures warmer than 273 K, mixed refers to temperatures between 273 and 238 K, and ice refers to temperatures below 238 K. ICS: In-Cloud Scavenging, BCS: Below-Cloud Scavenging, Sed and Dry Dep: Sedimentation and Dry Deposition.

Organic Matter	PF_init	CF_init	CF_pipe	CF_ed
Convective ICS				
Warm	14.3	12.0	11.1	12.5
Mixed	6.91	1.11	1.52	3.09
Ice	0.02	0.001	0.0009	0.001
Stratiform ICS				
Warm	20.9	23.9	25.0	25.5
Mixed	4.83	8.66	8.23	7.18
Ice	0.53	2.06	1.96	1.16
Stratiform BCS	10.6	11.7	11.8	10.2
Sed and Dry Dep	8.45	6.88	6.81	6.79

ACPD
12, 1687–1732, 2012

Table 7. Deposition budgets for dust (Tg yr^{-1}) for the four simulations presented in Table 2. Warm refers to cloud temperatures warmer than 273 K, mixed refers to temperatures between 273 and 238 K, and ice refers to temperatures below 238 K. ICS: In-Cloud Scavenging, BCS: Below-Cloud Scavenging, Sed and Dry Dep: Sedimentation and Dry Deposition.

Dust	PF_init	CF_init	CF_pipe	CF_ed
Convective ICS				
Warm	34.4	32.3	27.4	35.1
Mixed	31.6	2.99	4.08	9.15
Ice	0.16	0.01	0.02	0.05
Stratiform ICS				
Warm	26.8	41.6	42.5	43.0
Mixed	15.2	27.7	26.4	23.7
Ice	0.92	2.91	3.66	2.46
Stratiform BCS	171	192	209	225
Sed and Dry Dep	299	345	343	348

ACPD
12, 1687–1732, 2012

Table 8. Deposition budgets for sea salt (Tg yr^{-1}) for the four simulations presented in Table 2. Warm refers to cloud temperatures warmer than 273 K, mixed refers to temperatures between 273 and 238 K, and ice refers to temperatures below 238 K. ICS: In-Cloud Scavenging, BCS: Below-Cloud Scavenging, Sed and Dry Dep: Sedimentation and Dry Deposition.

Sea Salt	PF_init	CF_init	CF_pipe	CF_ed
Convective ICS				
Warm	348	624	678	455
Mixed	380	114	162	99.6
Ice	0.07	0.0002	0.0004	0.01
Stratiform ICS				
Warm	692	970	959	1050
Mixed	432	694	687	706
Ice	0.10	2.67	5.72	1.77
Stratiform BCS	1830	1450	1390	1570
Sed and Dry Dep	2550	2370	2310	2410

ACPD
12, 1687–1732, 2012

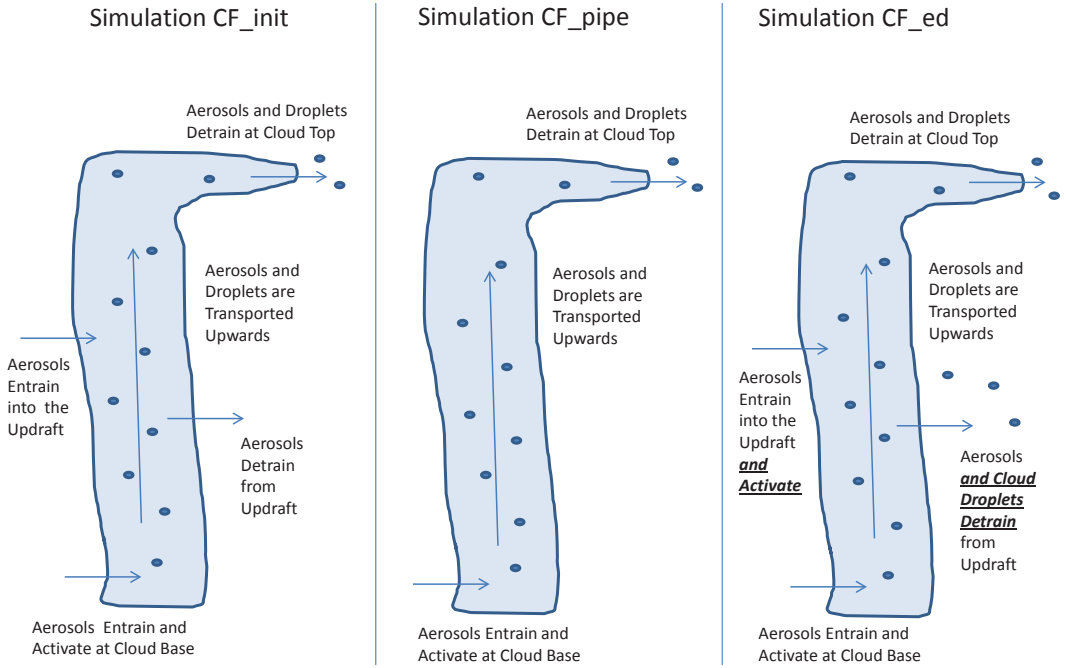

Fig. 1. Schematic showing the model setup in the convective updrafts for the three calculated cloud-droplet-borne/ice-crystal-borne aerosol fraction simulations. Simulations are also described in Table 2. Simulation PF_init has the same set-up as for simulation CF_init, except that the cloud-droplet-borne/ice-crystal-borne aerosol fractions are prescribed following Stier et al. (2005), not calculated based on the convective cloud microphysics of Lohmann (2008) as for the calculated fraction (CF) simulations.

ACPD
12, 1687–1732, 2012

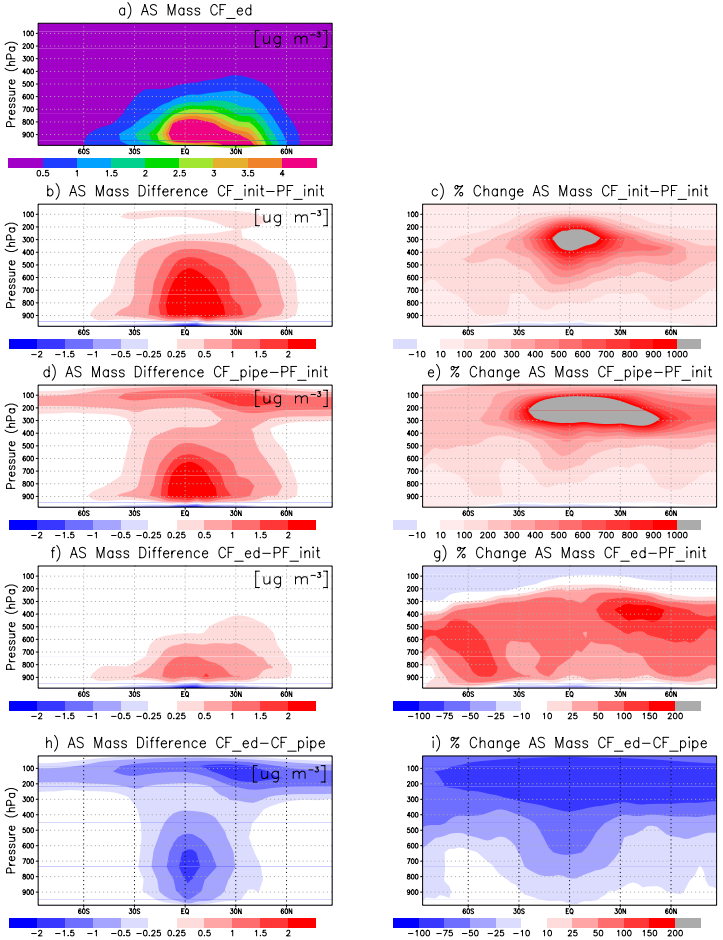

Fig. 2. The zonal and annual mean soluble/internally mixed accumulation (AS) mode mass concentration at STP for the simulation CF_ed (top panel), and the absolute and percent differences between the four simulations (remaining panels). All simulations are described in Table 2. The colorscales change between the different panels.

ACPD
12, 1687–1732, 2012

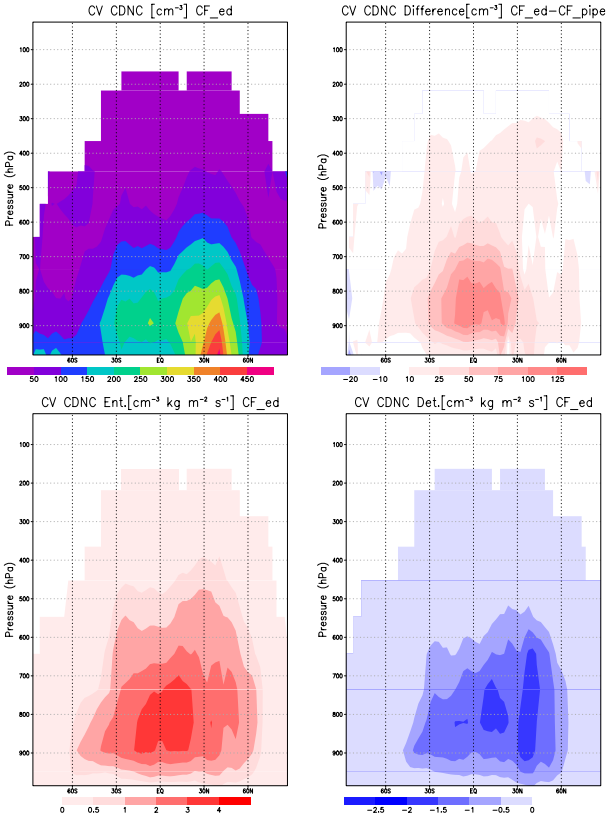

Fig. 3. The zonal and annual mean convective (CV) cloud droplet number concentration (CDNC) for the simulation CF_ed, and CV CDNC difference between the two limiting cases (CF_ed and CF_pipe) (top panels). The contribution of activated entrained aerosols to zonal and annual mean CV CDNC, and the reduction in the CV CDNC due to detrainment (bottom panels) (both multiplied by the vertical mass flux) for the simulation CF_ed. Simulations are described in Table 2.

ACPD
12, 1687–1732, 2012

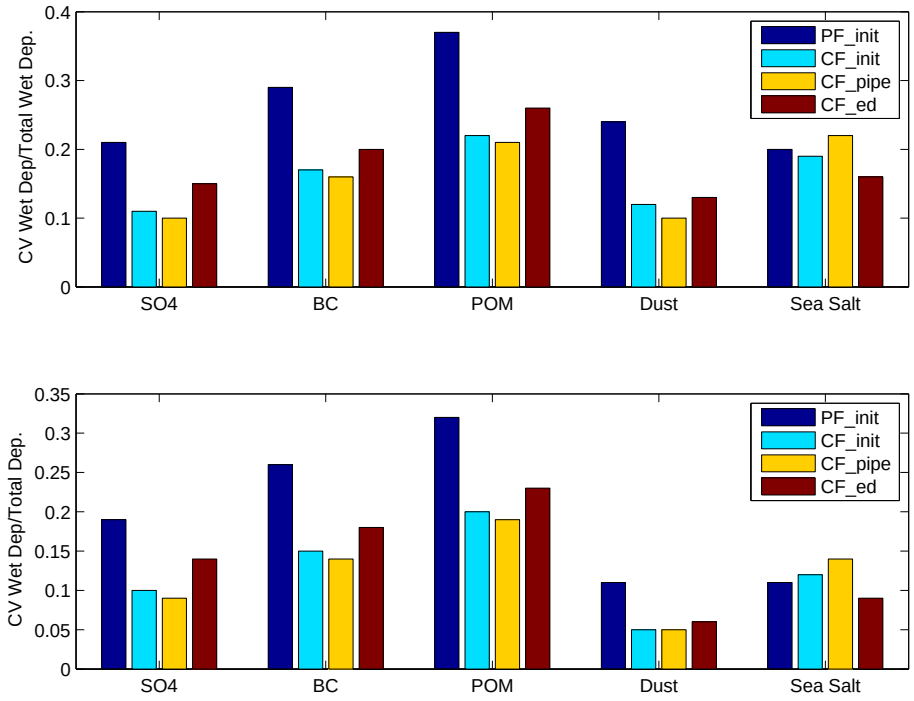

Fig. 4. The annual and global wet deposition attributed to convective (CV) precipitation relative to the total aerosol wet deposition attributed to both stratiform and convective precipitation (top panel), and the wet deposition attributed to convective (CV) precipitation relative to the total deposition (bottom panel) for each aerosol species (sulfate (SO_4), black carbon (BC), particulate organic matter (POM), dust and sea salt). Simulations are described in Table 2.

ACPD
12, 1687–1732, 2012

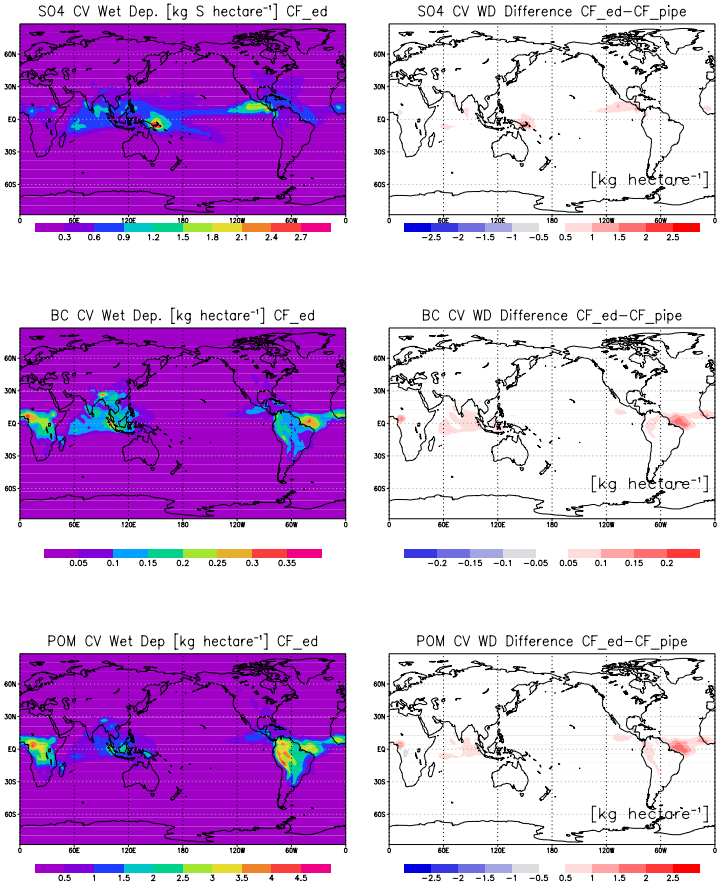

Fig. 5. The geographic distribution of annual mean convective wet deposition (CV Wet Dep.) for the simulation CF_ed and the absolute difference between CF_ed and CF_pipe for sulfate (SO_4), black carbon (BC) and particulate organic matter (POM). Simulations are described in Table 2.

ACPD
12, 1687–1732, 2012

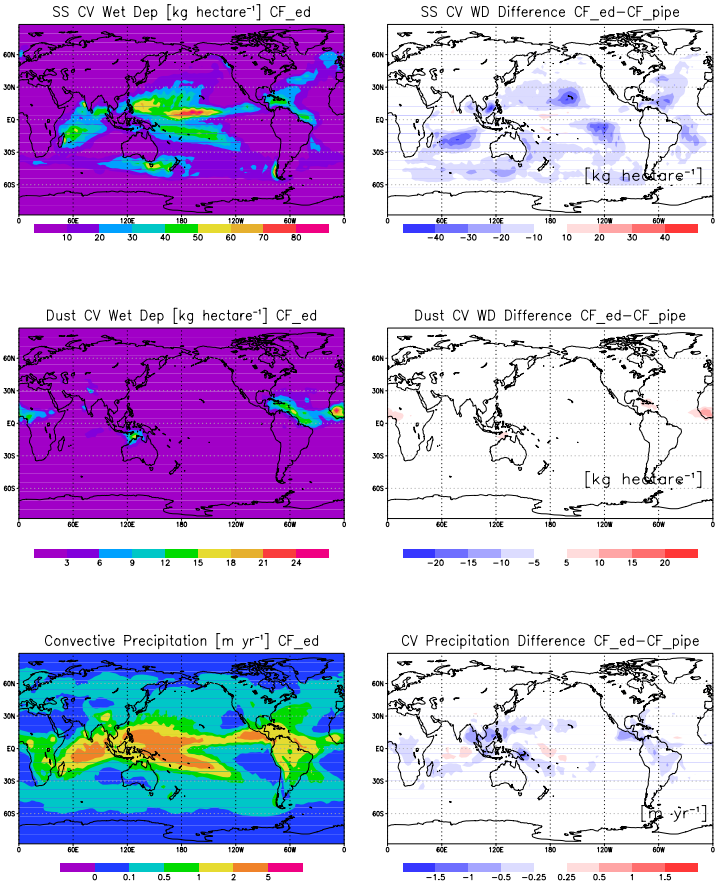

Fig. 6. The geographic distribution of annual mean convective wet deposition (CV Wet Dep.) for the simulation CF_ed and the absolute difference between CF_ed and CF_pipe for sea salt (SS) and dust, and the convective precipitation for simulation CF_ed and the absolute difference between CF_ed and CF_pipe. Simulations are described in Table 2.

ACPD
12, 1687–1732, 2012

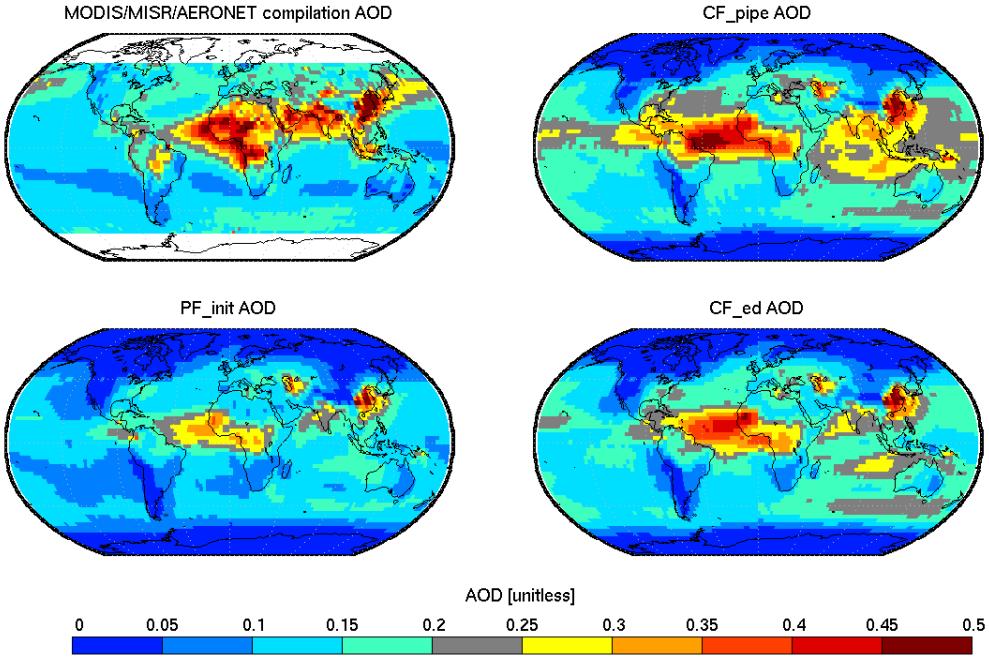

Fig. 7. The geographic distribution of aerosol optical depth (AOD) from the MODIS/MISR/AERONET compilation dataset of van Donkelaar et al. (2010) and for the simulations PF_init, CF_pipe, and CF_ed. The simulations are described in Table 2.

ACPD
12, 1687–1732, 2012

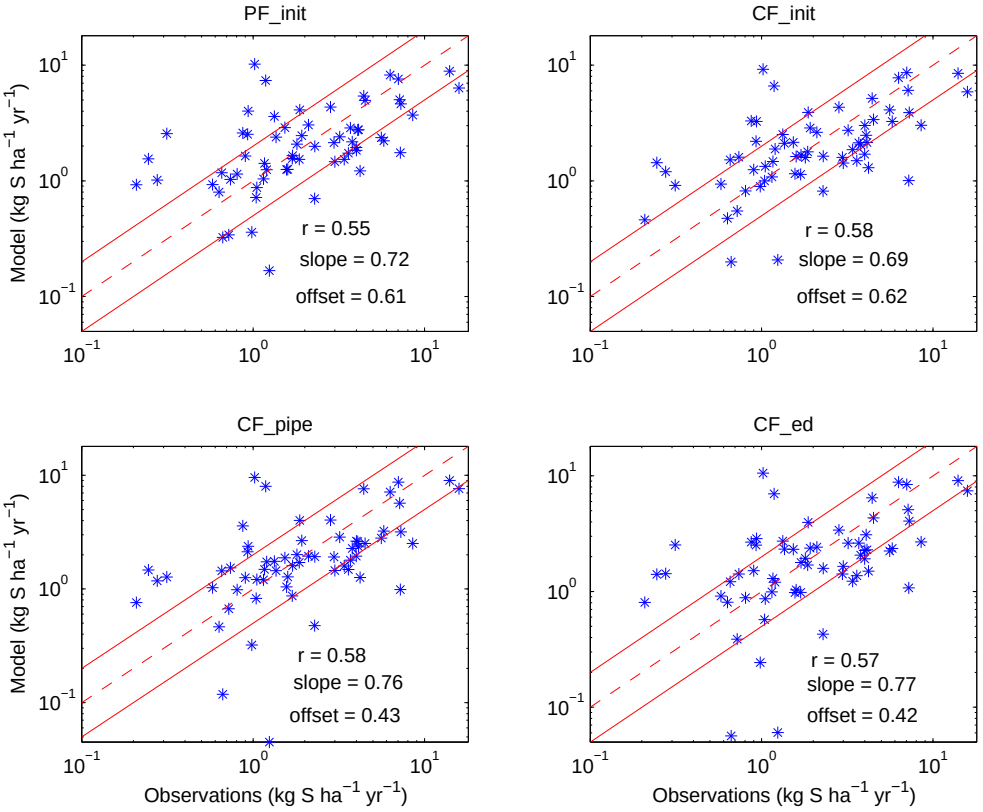

Fig. 8. Scatterplot of the observed and modeled wet deposition of sulfate from the dataset of Dentener et al. (2006a) (between 30° S and 30° N only) for the four simulations as described in Table 2.

ACPD
12, 1687–1732, 2012

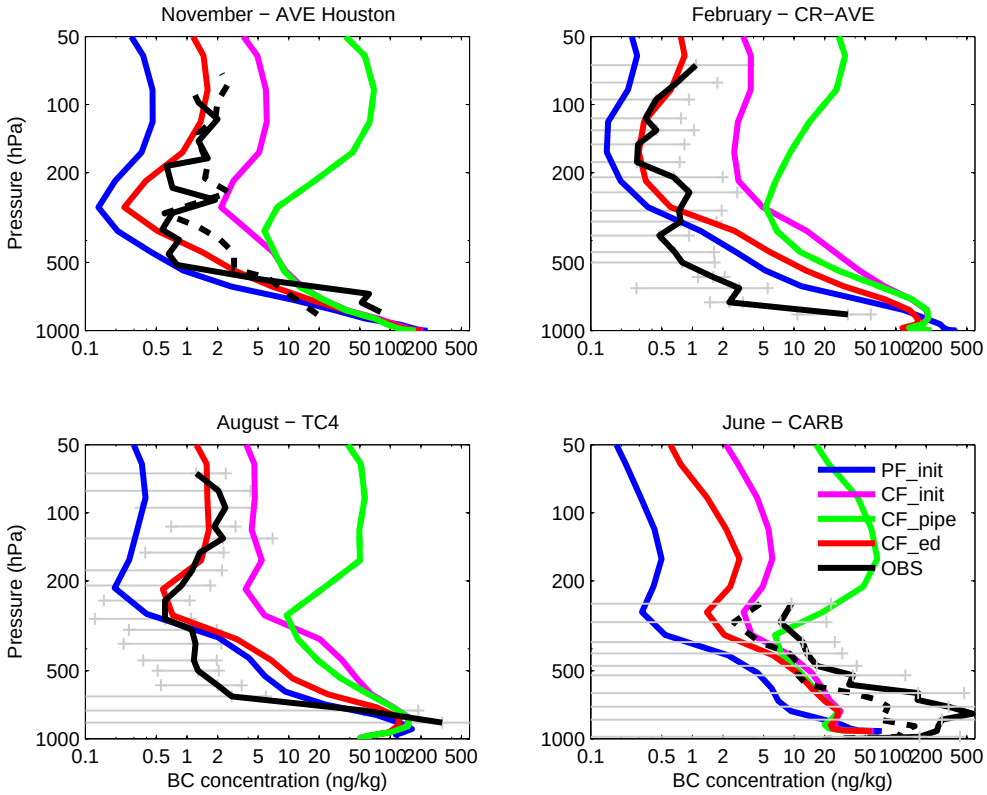

Fig. 9. Vertical profiles of black carbon (BC) concentration observations (OBS) from the aircraft data for tropical latitudes as described in Koch et al. (2009, 2010) and for the four simulation of this study as described in Table 2. Black dashed lines show observations from a different day of the aircraft campaign.

ACPD
12, 1687–1732, 2012